**Atmospheric
Chemistry
and Physics
Discussions**

Uncertainties of parameterized near-surface downward longwave and clear-sky direct radiation

S. Gubler, S. Gruber, and R. S. Purves

Department of Geography, University of Zurich, Zurich, Switzerland

Correspondence to: S. Gubler (stefanie.gubler@geo.uzh.ch)

Discussion Paper | Discussion Paper | Discussion Paper | Discussion Paper |

ACPD

12, 3357–3407, 2012

Uncertainties of parameterized near-surface LDR and SDR

S. Gubler et al.

Title Page

Abstract | Introduction

Conclusions | References

Tables | Figures

◄ | ►

◄ | ►

Back | Close

Full Screen / Esc

Printer-friendly Version

Interactive Discussion

Abstract

As many environmental models rely on simulating the energy balance at the Earth's surface based on parameterized radiative fluxes, knowledge of the inherent uncertainties is important. In this study we evaluate one parameterization of clear-sky incoming shortwave radiation (SDR) and diverse parameterizations of clear-sky and all-sky incoming longwave radiation (LDR). In a first step, the clear-sky global SDR is estimated based measured input variables and mean parameter values for hourly time steps during the year 1996 to 2008, and validated using the high quality measurements of seven Alpine Surface Radiation Budget (ASRB) stations in Switzerland covering different elevations. Then, twelve clear-sky LDR parameterizations are fitted to the ASRB measurements. One of the best performing LDR parameterizations is chosen to estimate the all-sky LDR based on cloud transmissivity. Cloud transmissivity is estimated using measured and modeled global SDR during daytime. For the night, the performance of several interpolation methods is evaluated.

Input variable and parameter uncertainties are assigned to estimate the total output uncertainty of the mentioned models, resulting in a mean relative uncertainty of 10 % for the clear-sky direct, 15 % for diffuse and 2.5 % for global SDR, and 2.5 % for the fitted all-sky LDR. Further, a function representing the uncertainty in dependence of the radiation is assigned for each model. Validation of the model outputs shows that direct SDR is underestimated (the mean error (ME) is around $-33\,\mathrm{W\,m^{-2}}$), while diffuse radiation is overestimated (ME around $19\,\mathrm{W\,m^{-2}}$). The root mean squared error (RMSE) scatters around $60\,\mathrm{W\,m^{-2}}$ for direct, and $40\,\mathrm{W\,m^{-2}}$ for diffuse SDR. The best behaviour is found, due to the compensating effects of direct and diffuse SDR, for global SDR with MEs around $-13\,\mathrm{W\,m^{-2}}$ and RMSEs around $40\,\mathrm{W\,m^{-2}}$. The ME of the fitted all-sky LDR is around $\pm10\,\mathrm{W\,m^{-2}}$, and the RMSE goes up to $40\,\mathrm{W\,m^{-2}}$. This is obtained by linearly interpolating the average of the cloud transmissivity of the four hours of the preceeding afternoon and the following morning.

1 Introduction

Incoming shortwave (SDR) and longwave radiation (LDR) strongly control the energy budget at the Earth's surface. They drive processes such as photosynthesis and evapotranspiration, and are therefore of great importance in hydrological or agricultural (Cooter and Dhakhwa, 1996), or energy technology studies (Schillings, 2004). Especially in view of climate change, the modeling of environmental processes has become important for the temporal and spatial estimation of changes and rates of change, and to improve the knowledge about the complex interactions between the atmosphere, the Earth surface and subsurface. In mountain areas, changes in the energy budget can already be observed at small distances due to the strong topographic variability.

Modeling the energy fluxes at the land surface as well as their uncertainties is a key step in any model application. A wide variation of models that estimate SDR or LDR have been proposed in the literature, ranging from complex physically-based models (e.g., MODTRAN) to empirical models based on relations between meteorological variables. For many applications, sophisticated models such as MODTRAN are inappropriate due to their complexity, required input and computational effort.

In this study, we investigate the behaviour of the clear-sky broadband radiation model by Iqbal (1983, based on Bird and Hulstrom, 1980, 1981), at seven locations in Switzerland. This model has been chosen since Gueymard (1993) has shown that it is among the four (out of the eleven they evaluated) models that reproduce direct and diffuse SDR best. Furthermore, the Iqbal model has been frequently used in many impact model applications (Corripio, 2002; Gruber, 2005; Machguth et al., 2008; Helbig et al., 2009) as well as other studies concerning the estimation of incoming solar radiation (Schillings, 2004). The model assumes a homogeneous atmosphere and uses an isotropic view factor approach. Due to these simplifications, input is limited to few quantities such as screen-level temperature, relative humidity and atmospheric pressure, and the model parameters consist of estimated ozone, aerosols and water vapour, among others, to determine the transmittance respectively scattering of the solar rays in the atmosphere.

One aim of this study is the quantification of the clear-sky Iqbal (1983) model uncertainties due to parameter and input uncertainty, and to validate the model output.

Many empirical parameterizations for the clear-sky LDR can be found in the literature (Brutsaert, 1975; Konzelmann et al., 1994). A further goal of this study is to calibrate some of the most often used parameterizations to local conditions in Switzerland, to assess the model errors and to identify the most appropriate parameterizations for further application. Since cloud cover is only rarely measured and measurements are error-prone, it is common to estimate the cloud transmissivity (resp. cloud cover) out of modeled and measured clear-sky global SDR during daytime. Measurements of global SDR are often available at meteo stations. The estimated cloud transmissivity is used to model the all-sky LDR. During the night, the cloud transmissivity is interpolated. We investigate diverse interpolation methods, and validate them by modeling the all-sky LDR.

The aims of the present study are:

- to estimate the output uncertainty of the clear-sky SDR model by Iqbal (1983) due to uncertainties in input variables and parameters,

- to evaluate the clear-sky Iqbal (1983) model at seven sites in Switzerland,

- to calibrate diverse clear- and all-sky LDR models,

- to assess the best all-sky LDR models for impact modeling studies in Switzerland,

- to study the output of different interpolation techniques of the cloud transmissivity during nighttime,

- and to estimate the output uncertainty of one all-sky LDR model.

All these steps are necessary to estimate the all-sky LDR and its associated uncertainties during day- and nighttime. To reach these aims, we firstly introduce the data and

the parameters necessary in the study. In Sect. 3, the methods to assess the sensitivity and the uncertainties in the clear-sky SDR model, and the validation and calibration methods are introduced. Then, the results are presented and discussed.

2 Data description

⁵ This modeling study is performed for seven locations in Switzerland (Fig. 1, Table 1). The model is run with measurements from MeteoSwiss (Sect. 2.1) and estimated parameters (Sect. 2.2). The uncertainties in the input data and the parameters were assigned based on expert knowledge and literature, or were estimated based on representative measurements. Perceptional and structural model errors (cf., Beck, 1987;
¹⁰ Beven, 1993; Kavetski, 2003; Gupta et al., 2005) are not investigated.

The data is structured as (a) input data, (b) physical and statistical model parameters and (c) validation data.

2.1 Input and validation data

The input data is obtained from the MeteoSwiss automatic meteorological network
¹⁵ (ANETZ). The Alpine Surface Radiation Budget (ASRB) (Philipona et al., 1996) network data serves for validation (SDR) and fitting (clear-sky and all-sky LDR). The number of study sites is restricted to the existence of both network stations. The study is performed with hourly data ranging from 1996 to 2008, resulting in 113976 data points. Since synoptic cloud observations are rare (they exist only for 3 stations of this study)
²⁰ and error-prone, clear-sky hours are estimated according to the cloud index by Marty and Philipona (2000). The measurement errors are assumed to be normally distributed with zero mean. The standard deviations (Table 2) were obtained from MeteoSwiss (courtesy of Rolf Philipona, Philipona et al., 1995). All measured data is denoted with [*].

2.2 Physical and statistical model parameters

2.2.1 Global SDR

The main focus of this study lies on the estimation of uncertainty due to the absorption, scattering and transmittance of the sun rays in the atmosphere, plus their reflection at the ground surface for the Iqbal (1983) model. The model is hereafter referred to as the Iqbal model. The uncertainties in the ozone column data, the visibility, the precipitable water and in the ground albedo are investigated. Uncertainties due to Rayleigh-scattering are included by the uncertainty in the relative optical air mass. Mean and standard deviation of the mentioned parameters are estimated using measurements recorded in Switzerland, which are mostly available at a daily or even less frequent resolution.

Visibility: Visibility is used to parameterize attenuation due to aerosols (Eq. A11). Visibility is manually recorded five times per day at the Jungfraujoch by MeteoSwiss. The data ranges from 0 km to 75 km. To estimate the probability density function (PDF) of the visibility, two assumptions are made: a) low visibility (i.e. less than 5 km) are mainly caused by foggy situation, snow storms or clouds, and not by a high aerosol concentration in the atmosphere. Therefore, all values less than 5 km were deleted. The second assumption b) is that the visibility can be larger than 75 km on very clear days in fall or winter. The upper limit of the distribution is set to 120 km, resulting in a truncated normal distribution.

Water vapor: The effect of absorption due to water vapor contained in the atmosphere is estimated using the precipitable water w (Eq. A10). The precipitable water is the height (cm) of the column of water at the Earth's surface, if all the water vapor in zenith direction was condensated. Data of precipitable water is only rarely available (Iqbal, 1983), and is thus often parameterized. Historical overviews of precipitable water parameterizations are given in Iqbal (1983) and Okulov et al. (2002). Here, the

parameterization found in Reitan (1963); Leckner (1978) and Prata (1996) is used:

$$w = a_w \frac{h_r^* p_s}{T^*}, \tag{1}$$

where a_w is estimated, h_r^* is the measured relative humidity in fractions of one, p_s is saturated vapor pressure in hPa and T^* is screen-level temperature in K. The vapor pressure in saturated air is determined as a function of air temperature (Flatau et al., 1992). The parameter a_w [g K hPa^{-1} cm^{-2}] is estimated as (Prata, 1996):

$$a_w = \frac{M_w}{R \cdot k \cdot \psi}, \tag{2}$$

where $M_w = 18.02$ g mol^{-1} is the molecular weight of water vapor, $R = 8.314$ J K^{-1} mol^{-1} is the universal gas constant and $\psi = 1.006$ is a constant. Further, $k = k_w + \frac{\gamma}{T^*}$, where $k_w = 0.44$ km^{-1} is the inverse water vapor scale height (Reitan, 1963; Brutsaert, 1975) and γ is the lapse rate. The uncertainty of a_w is estimated by propagating the uncertainty inherent in the air temperature measurements and the lapse rate. The lapse rate is assumed to be normally distributed with mean equal to the standard value of -6.5 °K km^{-1} for the Alps and standard deviation of 1 °K km^{-1}, based on the investigations of Hebeler and Purves (2008). Following the investigations of Foster et al. (2006), a_w and w are assumed to be lognormally distributed.

Ozone: MeteoSwiss provides accurate ozone column measurements in Arosa (Staehelin et al., 1998) at about two thirds of all days during the year. Ozone is assumed to be lognormally distributed.

Relative optical air mass: The formula of the relative optical air mass (Eq. A5) is accurate to better than 0.1 % for zenith angles of up to 86° (Iqbal, 1983). This relative uncertainty was multiplied to all zenith angles from one to ninty degrees. It resulted that the mean absolute uncertainty of the relative optical air mass is 0.03. The error in the relative optical air mass is assumed to be normally distributed with zero mean and standard deviation 0.03.

Ground albedo: Ground albedo measurements for each of the study sites were obtained from the "MODIS/Terra + Aqua BRDF and Calculated Albedo" data set (ORNL DAAC, 2010). Ground albedo is assumed to be lognormally distributed (Oreopoulos and Davies, 1998; Mulrooney and Matney, 2007), with an upper cut-off at one. Due to the strong temporal and spatial variability of ground albedo, the measurements are separately examined for each study site and each month of the year (Table 7).

2.2.2 LDR

The LDR parameterizations contain statistical parameters (Table 3). Originally, they were fitted to measurements at specific research areas. In this study, we fit the selected parameterizations to the measurements at the seven study sites in Switzerland, and identify reliable parameter values for the local conditions. The confidence intervals of the non-linear least squares parameter estimation are used to quantify the uncertainty of the parameters.

3 Methods

3.1 Model formulations

In this section, we give a brief overview of the model formulations and parameterization used in this study.

3.1.1 Clear-sky SDR

In a first step, the clear-sky broadband global SDR is estimated (Iqbal, 1983, Model C). For details the reader is asked to check Appendix A. The model estimates the direct SDR by calculating the radiation at the top of the atmosphere (Corripio, 2002), and the attenuation of the sun rays by ozone, water vapour, aerosol and dry-air particles in the atmosphere. Then, the diffuse SDR due to Rayleigh-scattering, scattering by

aerosols and water vapour and the multiple reflection of the sun rays between the Earth's surface and the atmosphere is estimated. Direct and diffuse radiation sum up to the global SDR. Radiation due to scattering from surrounding terrain is included. However, it only accounts for a very small part of the total global SDR since the study locations are situated in flat terrain.

3.1.2 Clear-sky LDR

The clear-sky LDR is determined by the Stefan-Boltzmann law, i.e. by the bulk emissivity e_{atm} and the effective temperature of the overlying atmosphere, i.e.:

$$LDR_{cl} = e_{atm} \cdot \sigma_{SB} \cdot T_{atm}^4, \tag{3}$$

where $\sigma_{SB} = 5.67 \times 10^{-8}\,\mathrm{W\,m^{-2}\,K^{-4}}$ denotes the Stefan-Boltzmann constant, e_{atm} the bulk emissivity and T_{atm} the effective temperature of the overlying atmosphere. In practice, T_{atm} is replaced by the temperature at screen-level height temperature T and the atmospheric emissivity:

$$LDR_{cl} = e_{cl}(e, T^*) \cdot \sigma_{SB} \cdot T^{*4}, \tag{4}$$

where T^* denotes absolute air temperature (K) at the reference height of 2 m above the ground and e_{cl} is the clear-sky emissivity. The clear-sky emissivity parameterizations are based on statistical relationships between the emissivity, temperature and vapour pressure $p_v = h_r \cdot p_s$ (Table 3). Note that the parameterization presented by Dilley and O'Brien (1997) is not based on the Stefan-Boltzmann law.

3.1.3 Cloud transmissivity and clouds

The amount of clouds in the atmosphere determines the difference between clear-sky and all-sky LDR. Since cloud observations only rarely exist, it is a common use

to estimate the cloud transmissivity τ_c by comparing the estimated clear-sky global SDR_{glob} with the measured global radiation SDR^*_{glob} (Greuell et al., 1997):

$$\tau_c = \frac{SDR^*_{glob}}{SDR_{glob}}. \qquad (5)$$

Note that $\tau_c < 1$ if the sky is overcast, and $\tau_c = 1$ denotes clear-sky conditions. Most of the parameterizations for the all-sky LDR are based on the cloud-factor N, which is zero if the sky is completely clear, and one if the sky is cloud-covered. A simple relation between τ_c and N was proposed by Crawford and Duchon (1998):

$$\tau_c = 1 - N. \qquad (6)$$

In this study however, the cloud transmissivity τ_c is used directly, instead of N, to estimate the all-sky LDR in this study.

3.1.4 All-sky LDR

The all-sky parameterizations using the cloud cover N are based on studies by Pirazzini et al. (2001).

$$LDR_{all} = LDR_{cl} \cdot (1 + a\, N^{p_0}) \qquad (7)$$

and

$$LDR_{all} = (\epsilon_{cl}(1 - N^{p_1}) + \epsilon_{oc}N^{p_2})\sigma_{SB}T^{*4}, \qquad (8)$$

where ϵ_{cl} is the estimated clear-sky emissivity, a, p_0, p_1 and p_2 are parameters and ϵ_{oc} is the cloud emissivity. To avoid the step of transforming the cloud transmissivity to cloud cover (Eq. 6), the parameterizations are slightly modified and then fitted to τ_c instead of N. The resultant equations are:

$$LDR_{all} = LDR_{cl} \cdot (1 + \tilde{a}\,(1 - \tau_c)^{\tilde{p}_0}), \qquad (9)$$

and

$$LDR_{all} = (\epsilon_{cl} \cdot \tau_c^{\tilde{p}_1} + \epsilon_{oc}(1 - \tau_c^{\tilde{p}_2}))\sigma_{SB}T^{*4}. \tag{10}$$

In addition to the modified Pirazzini et al. (2001) parameterizations, the two power expressions of τ_c in Eq. (10) were replaced by polynomials in τ_c of orders $n = 1, 2, ..., 6$ and a constant of value zero, resulting in:

$$LDR_{all} = (\epsilon_{cl} \cdot (a_1\tau_c + \cdots + a_n\tau_c^n) + \epsilon_{oc}(1 - (a_1\tau_c + \cdots + a_n\tau_c^n)))\sigma_{SB}T^{*4}. \tag{11}$$

3.2 Sensitivity analysis

Local sensitivities of direct, diffuse and global clear-sky SDR to ozone, precipitable water, visibility and ground albedo are estimated. The sensitivities are estimated for constant path length $m_r = 4.3$, the mean path length estimated at Jungfraujoch. Each model parameter θ_i is varied within the interval $[\mu_i - 3\sigma_i, \mu_i + 3\sigma_i]$, while all other parameter $\theta_{j \neq i}$ are kept fixed at μ_j. Thereby, the influence of 99 % of the most plausible parameter values on the SDR is investigated.

3.3 Uncertainty assessment

Monte-Carlo based methods are widely used to derive the probability density function (PDF) of the output of a model due to the simple implementation even for complex, non-linear models. In a first step, the input and the parameter uncertainty are estimated (Sect. 2). Thereby, a PDF (often called prior distribution) is assigned to each input variable and each parameter of interest. To reduce complexity and simulation cost, input variables and parameters are often pre-selected based on preliminary analyses such as sensitivity studies. In the present case, the number of variables/parameters was sufficiently small to be evaluated completely. The parameters and the input variables are sampled from their respective prior distributions (Table 2). Uncertainties in the parameters and input data are assumed to be independent. 10 000 model realizations are performed in this study. Statistical parameters such as the mean, the standard

deviation and the 2.5 %- and 97.5 %-quantiles of the simulation outputs are estimated. The 95 %-confidence interval for timestep t is $CI_t := [q_{0.025}(y_t), q_{0.975}(y_t)]$. The standard uncertainty of the model is defined as the standard deviation $\sigma_{t,abs}$ of the model result at each time step (JCGM, 2008). The relative uncertainties are $\sigma_{t,rel} = \sigma_{t,abs}/\mu_t$. To derive the relative uncertainty in dependence of the modeled radiation (i.e., a function $\sigma_{SDR_{dir},rel} = f(SDR_{dir})$ in the case of direct SDR), a function f is fitted to the relative uncertainties using non-linear least-squares regression.

3.4 Validation

The model outputs are validated with the ASRB data (Sect. 2.1). The validation measures are assessed for a simulation with fixed inputs (no error) and fixed parameters (the mean in Table 2). A typical estimate to assess the validity of a model output[1] is the root mean squared error (RMSE) which accounts for the average magnitude of the errors, puts weight on larger errors, but does not account for the direction of the errors:

$$RMSE = \sqrt{\frac{1}{n}\sum_{t=1}^{n}(y_t - y_t^*)^2},$$

$$RMSE \in [0, \infty), \ RMSE_{perf} = 0. \tag{12}$$

The mean error ME is a simple and very familiar measure that neglects the magnitude of the errors (i.e. positive errors can compensate for negative ones):

$$ME = \frac{1}{n}\sum_{t=1}^{n}(y_t - y_t^*)$$

$$ME \in (-\infty, \infty), \ ME_{perf} = 0. \tag{13}$$

---

[1]The definitions and explanations of the validation estimates are from http://www.cawcr.gov.au/projects/verification/verif_web_page.html#Standard_verification_methods.

3368

The correlation coefficient R measures the linear agreement between the modeled and the measured variable:

$$R = \frac{\sum_{t=1}^{n}(y_t - \overline{y})(y_t^* - \overline{y^*})}{\sqrt{\sum_{t=1}^{n}(y_t - \overline{y})^2(y_t^* - \overline{y^*})^2}}$$

$$R \in [-1, 1], \ R_{\text{perf}} = 1, \tag{14}$$

The coefficient of determination R^2 indicates the amount of variation in one variable explained through the other.

Further, the number of hits are estimated to indicate whether the true value (or in this case the measurement) lies within the 95 %-confidence intervals of the model output. The uncertainty interval of the measured output is $CI_t^* := [y^*(1 - 2\sigma_{y^*}), y^*(1 + 2\sigma_{y^*})]$, where y^* is the measured output variable and σ_{y^*} is the measurements precision defined in Table 2. The hit function $h(t)$ is defined as:

$$h(t) = \begin{cases} 1, \text{ if } CI_t \cap CI_t^* \neq \emptyset, \\ 0, \text{ else}. \end{cases} \tag{15}$$

The relative hits are defined as the fraction of the number of hits and the total number of simulation time steps. The hits measure the probability (as a relative frequency) that the real value lies within the estimated uncertainty interval of the simulation output.

3.5 Non-linear least squares estimation

A nonlinear least-squares method (Bates and Watts, 1988; Bates and Chambers, 1992) is used to fit the clear-sky LDR parameterizations (Table 3) to observational data (ASRB). In a first step, the clear-sky emissivity is estimated as:

$$\epsilon_{\text{cl}} = \frac{\text{LDR}_{\text{in,cl}}^*}{\sigma_{\text{SB}}T^{*4}}, \tag{16}$$

where both $\text{LDR}^*_{\text{in,cl}}$ and T^* are measurements of the ASRB stations. Then, the parameters of the parameterizations in Table 3 are fitted to e_{cl}. The start values for the nonlinear estimation are the parameters presented in the respective publications. The clear-sky situations are separated from the all-sky situations using Dürr and Philipona

5   (2004). Thereby, parameter values for each station are obtained. Furthermore, the parameterizations are fitted simultaneously to all stations, resulting in one optimal parameter value.

In a next step, the behaviour of the different parameterizations is evaluated according to four criteria: a) small mean error (in absolute terms, Eq. 13), b) small root mean

10 squared error (Eq. 12), c) similarity in order of magnitude of parameter estimates and published values and d) convergence of the nonlinear regression model at all locations. According to these four criteria, the best parameterizations are identified.

Similarily, the all-sky LDR (Eqs. 9, 10 and 11) are fitted and evaluated for all daytime hours.

15 **3.6   Interpolation of cloud transmissivity during nighttime**

The cloud transmissivity can, during daytime, be estimated by the comparison of modeled and measured global radiation (Eq. 5). During the night, it is often linearly interpolated between the last point in time at sunset, and the first point in time in the morning, or the constant interpolation taking a mean cloud amount value from the precedent

20 afternoon (Lhomme et al., 2007). However, these estimates are rarely validated due to the lack of available data. Here, we use different interpolation techniques to estimate the cloud transmissivity during nighttime, estimate the all-sky LDR and evaluate the outputs with the ASRB measurements.

The interpolation methods we study are:

25 1. linear interpolation between a mean value of x points in time (where each point in time represents an hourly value) before sunset and x points in time after sunrise,

2. constant interpolation of the mean value of x points in time before sunset,

3. constant interpolation of the mean value of x points in time after sunrise,

where $x \in \{1, \ldots, 6\}$.

4   Results

4.1   SDR

4.1.1   Validation

Validation measures are estimated for one simulation performed with the mean values μ of all parameters and input variables (Table 2). Only clear-sky hours were considered for validation, the results are presented in Table 4 and Fig. 2.

The RMSE scatters around $61\,\mathrm{W\,m^{-2}}$ for direct, around $41\,\mathrm{W\,m^{-2}}$ for diffuse and $40\,\mathrm{W\,m^{-2}}$ for global radiation. The mean error of the direct radiation is negative at all locations, indicating a general under-estimation of the direct radiation by the model, similar for the global radiation with the exception of the two lowest sites Locarno Monti and Payerne. The correlations with elevation are negative for direct, diffuse and global radiation, and the values scatter around $-33\,\mathrm{W\,m^{-2}}$ for direct, around $19\,\mathrm{W\,m^{-2}}$ for diffuse and around $-13\,\mathrm{W\,m^{-2}}$ for global SDR. The R^2-value is in general very high for direct and global radiation, indicating a good linear relation between the modeled and the measured values (Fig. 2). However, the fit for the diffuse SDR is poor, with a strong over-estimation of the diffuse radiation for values around $50\,\mathrm{W\,m^{-2}}$ to $100\,\mathrm{W\,m^{-2}}$. Further, we see that the modeled clear-sky diffuse radiation reaches a limit of around $120\,\mathrm{W\,m^{-2}}$. This might be attributed to the high visibility adopted from Jungfraujoch. Similiar studies (Gueymard, 1993) show higher limits for the diffuse radiation assuming higher aerosol contents.

In general, global SDR performs best for these validation measures, resulting in smallest RMSE and ME (as absolute value) for all sites, since the positive errors for diffuse radiation at low elevation sites compensate for the negative errors in direct

radiation. At the high elevation sites, the under-estimation of direct radiation is not compensated by the diffuse radiation, in contrast to the low elevation sites. This can, on one hand, be attributed to the fact that the under-estimation of direct radiation is stronger at high elevation sites, and on the other hand that the over-estimation of diffuse radiation is less pronounced at the high elevation sites.

To check whether the errors $e_t := y_t - y_t^*$ systematically depend on either input variables or the sun elevation, they were correlated with the input variables relative humidity, air temperature and pressure, and the sun elevation. The correlations are low for all input variables (at most 0.2). Further, a multiple linear model consisting of all mentioned variables was fitted to the respective errors. Again, high correlations were not observed.

One restriction of this validation must be kept in mind: the estimation of the clear-sky days is based on the cloud estimation of Dürr and Philipona (2004) and therefore error-prone. We therefore additionally estimated the validation measures for clear-sky days using the synoptic cloud observations at the three stations Jungfraujoch, Payerne and Locarno-Monti. Since the overall picture of the validation measures did not differ much from the first analysis, the results of the clear-sky validation presented here are assumed to be reliable. A further indication of the validity of the Dürr and Philipona (2004) validation results is that the errors in the modeled clear-sky radiation do not correlate with the observed cloud cover.

4.1.2 Sensitivity of the clear-sky SDR

Direct and diffuse SDR are most sensitive to visibility, with a stronger sensitivity if the visibility reaches only few kilometers. The reaction of modeled direct and diffuse SDR on visibility has an opposite sign (Fig. 3). High visibility implies more direct radiation due to less absorption by aerosols. In constrast, few aerosols reduce the diffuse SDR due to less scattering. Since in the sum, the effects on direct and diffuse radiation are compensated, global radiation is, in relative terms, less sensitive to visibility. Further, precipitable water is a sensitive parameter, resulting in more than 30 % differences in

SDR. For global radiation, the sensitivity to precipitable water is of the same order of magnitude as the sensitivity to ground albedo, but opposite. The sensitivity to either ozon is almost negligible (resulting in around 1 % difference) for direct and diffuse radiation. The diffuse radiation is very sensitive to ground albedo. Since the diffuse fraction accounts only for a small part of the total clear-sky global SDR, the sensitivity to ground albedo is less pronounced for global SDR.

4.1.3 Uncertainty

The uncertainties for direct, diffuse and global SDR are shown in Fig. 4. Uncertainty in direct SDR increases with decreasing elevation, as there is a clear positive correlation of uncertainty with the path length. No such pattern can be observed for diffuse and global radiation. The 95 %-quantile of the absolute standard deviation of all time steps for the direct SDR goes from $28\,\mathrm{W\,m^{-2}}$ (JUN) to $35\,\mathrm{W\,m^{-2}}$ (OTL), and is smaller for the diffuse radiation ($23\,\mathrm{W\,m^{-2}}$). The smallest standard deviation is observed for global radiation (around $12\,\mathrm{W\,m^{-2}}$), resulting from the compensating effects of modeled direct and diffuse radiation. The relative uncertainty for direct radiation approximates 5 % with increasing radiation. The mean value of the relative uncertainties of the direct radiation does not exceed 10 % at all stations, however the 95 %-quantile of the relative uncertainties is 20 %. For diffuse radiation, the 95 %-quantile is 20 %, the mean value scatters around 15 %. The 95 %-quantiles of the standard deviations of global radiation do not exceed 10 %, while the mean value scatters around 2.5 %. A conservative estimate (i.e. towards higher uncertainty) of the uncertainty in SDR is:

$$SDR_i = SDR_i^{est} \cdot (1 + \varepsilon_{i,SDR}), \tag{17}$$

with

$$\varepsilon_{i,SDR} \sim \begin{cases} \mathcal{N}(0,0.2), & \text{if } i = \text{direct}, \\ \mathcal{N}(0,0.2), & \text{if } i = \text{diffuse}, \\ \mathcal{N}(0,0.1), & \text{if } i = \text{global}, \end{cases} \tag{18}$$

3373

while a more confident estimate results in:

$$\varepsilon_{i,\text{SDR}} \sim \begin{cases} \mathcal{N}(0,0.1), & \text{if } i = \text{direct}, \\ \mathcal{N}(0,0.15), & \text{if } i = \text{diffuse}, \\ \mathcal{N}(0,0.025), & \text{if } i = \text{global}. \end{cases} \tag{19}$$

Further, a function $f(\text{SDR}) = \sigma_{\text{SDR,rel}}$ was fitted through the relative uncertainties for all three radiation types using non-linear least-squares estimation, resulting in:

$$\sigma_{\text{SDR}_i,\text{rel}} = \begin{cases} 1.25 - \frac{1}{\text{SDR}_i^{-0.029}}, & \text{if } i = \text{direct}, \\ 0.034 + 0.013\sqrt{\text{SDR}_i}, & \text{if } i = \text{diffuse}, \\ 1.07 - \frac{1}{\text{SDR}_i^{-0.008}}, & \text{if } i = \text{global}. \end{cases} \tag{20}$$

In addition to the validation measures presented in Sect. 4.1.1, the relative hits were estimated for all solar elevations in steps of 1° (Fig. 5). The direct SDR behaves well (in more than 50 % of the cases) at all stations for solar elevations greater than 40°, where in general the lower elevation stations perform more satisfactorily. A trend with elevation can be observed for the diffuse radiation: modeled diffuse radiation performs better for stations at higher elevations (Table 4). In general, the model over-estimates the diffuse radiation. For global radiation, a clear distinction is observed for the high and the low elevation sites: while for the second, the number of hits are high for sun elevations of more than 30°, the model performs poor at the high elevation sites, where global radiation is mostly under-estimated. In general, the model performs poor for low sun elevations, resulting in relative hits of less than 20 % for sun elevations lower than 30°. This result plus the fact that the hits for global radiation are worse than for direct radiation is also coupled to the smaller uncertainties at low sun elevation or in global radiation in comparison to high sun elevations or direct radiation. The uncertainty for global SDR at all stations lies between $5\,\text{W}\,\text{m}^{-2}$ and $10\,\text{W}\,\text{m}^{-2}$, which is about half or one third of the uncertainty in direct SDR (Fig. 4). Achieving a hit for global SDR is therefore harder than for direct SDR, explaining the poor behaviour of the high elevation sites. The results for the relative hits can therefore only be regarded in dependence of

Title Page

Abstract | Introduction

Conclusions | References

Tables | Figures

|◄ | ►|

◄ | ►

Back | Close

Full Screen / Esc

Printer-friendly Version

Interactive Discussion

the results of the total output uncertainty. The low hits for global SDR either indicate a missing source of model uncertainty, or poor model performance.

4.2 LDR

4.2.1 Parameter estimation and validation of the clear-sky LDR

The non-linear least-squares fitting of the clear-sky LDR parameterizations (Table 3) to the seven stations in Switzerland resulted in the parameter values presented in Table 5. For most parameterizations, a clear trend of the estimates is observed with elevation, indicating that a linear function of the parameters with elevation would result in an improvement of the parameterizations. Since for many modeling applications, a modeler only uses one parameter estimate, the parameterizations were further fitted to all stations simultaneously.

For a comparison of the behaviour of the estimated parameters, the ME and the RMSE of the clear-sky LDR of the published parameterizations were estimated in a first step. Except for the Brunt (1932); Iziomon et al. (2003); Plüss and Ohmura (1996) and Konzelmann et al. (1994) all parameterizations perform well, with MEs ranging from around $-10 \, \mathrm{W\,m^{-2}}$ to $60 \, \mathrm{W\,m^{-2}}$, and RMSEs ranging from $10 \, \mathrm{W\,m^{-2}}$ to $60 \, \mathrm{W\,m^{-2}}$. The ME of the worst parameterizations (Brunt, 1932; Plüss and Ohmura, 1996; Konzelmann et al., 1994; Iziomon et al., 2003) go from $60 \, \mathrm{W\,m^{-2}}$ to more than $300 \, \mathrm{W\,m^{-2}}$ in absolute values, similar the RMSE. The Konzelmann et al. (1994) parameterization shows an ME of $-80 \, \mathrm{W\,m^{-2}}$ and a RMSE of $80 \, \mathrm{W\,m^{-2}}$, similar as shown by Pirazzini et al. (2001, Table 1). This can be explained by the unit of the water vapor pressure, which is (in Pirazzini et al. (2001) among others) assumed to be in hPa. Konzelmann et al. (1994) however fitted the parameterization using Pascal as the unit of water vapor pressure. By doing so, the ME and RMSE reduce to $30 \, \mathrm{W\,m^{-2}}$. To avoid confusion, the unit of water vapor pressure is always hPa in this work. Therefore, water vapor pressure p_v is multiplied by one hundred in the Konzelmann et al. (1994)-parameterization (Table 3).

For validation, the parameters estimated for each station individually are analysed.

The ME of these estimates does not exceed $1.5\,\mathrm{W\,m^{-2}}$ for all parameterizations and locations. The RMSE scatters between $6\,\mathrm{W\,m^{-2}}$ and $12\,\mathrm{W\,m^{-2}}$ for the so-called "well-behaving" parameterizations (Dilley and O'Brien, 1997; Brutsaert, 1975; Konzelmann et al., 1994), and goes up to $18\,\mathrm{W\,m^{-2}}$ for the simple Maykut and Church (1973) param-

5 eterization, which assumes the clear-sky emissivity being a constant. In general, the ME and the RMSE were strongly reduced by the parameter fitting in comparison to the published values. Among all tested parameterizations, the Dilley and O'Brien (1997) parameterization performs best in order of the validation measures RMSE and ME. Furthermore, Idso and Jackson (1969) has a small ME, however the RMSE is large.

10 Idso (1981) shows a small ME for the low elevation sites, however for the higher sites, the ME is larger than for other parameterizations, similar its RMSE. Brutsaert (1975); Konzelmann et al. (1994); Angström (1918); Dilley and O'Brien (1997) and Brunt (1932) perform relatively similar, with larger ME and RMSE at the low elevation sites. All parameterizations were analysed according to their ME, RMSE, the order of magnitude of

15 the estimated parameters and their convergence for all elevations. Thereby, it results that the Brutsaert (1975); Konzelmann et al. (1994); Dilley and O'Brien (1997) and the Angström (1918) parameterizations are among the best. For the proximity of a potential linear regression line to the diagonal, these parameterizations together with Brunt (1932) perform best.

20 In a next step, the parameterizations fitted to all stations simultaneously (Table 5) are analysed. Similarly, the best behaving parameterizations are Brutsaert (1975); Konzelmann et al. (1994); Angström (1918); Dilley and O'Brien (1997) and Brunt (1932), for which the ME ranges between $-5\,\mathrm{W\,m^{-2}}$ and $6\,\mathrm{W\,m^{-2}}$, and the RMSE does not exceed $12\,\mathrm{W\,m^{-2}}$. Among them, Dilley and O'Brien (1997) has the smallest RMSE ($10\,\mathrm{W\,m^{-2}}$).

25 Since the performance of the best behavioural parameterizations is very similar, only one of the parameterizations was further studied to fit the all-sky LDR parameterization. Konzelmann et al. (1994) is preferred over the other well-behaving parameterization since apparently the use of only two parameters is sufficient to model clear-sky emissivity. Further, it is preferred over the even "simpler" parameterization (in terms of

Title Page

Abstract | Introduction

Conclusions | References

Tables | Figures

◄ | ►

◄ | ►

Back | Close

Full Screen / Esc

Printer-friendly Version

Interactive Discussion

number of parameters) by Brutsaert (1975), since Konzelmann et al. (1994) includes the additive constant representing the clear-sky emissivity of a dry atmosphere to include the effect of greenhouse gases.

4.2.2 Parameter estimation and validation of the all-sky LDR during daytime

The parameterizations of all-sky LDR are based on an estimated clear-sky emissivity coupled with the effect of cloudiness or cloud emissivity. Clear-sky emissivity is estimated according to Konzelmann et al. (1994) with the fitted parameter estimates (Table 5) during daytime. The fit was performed with the values of the clear-sky LDR fits for all station simultaneously. The fitted values of the parameters of the two (modified) parameterizations found in Pirazzini et al. (2001) are presented in Table 6. Except for Cimetta, where the estimate of ϵ_{oc} is slightly larger than one ($0 \leq \epsilon_{oc} \leq 1$ represents the cloud emissivity), all parameters have values that are comparable with the ones found in the literature (Pirazzini et al., 2001, c.f. Table 3). We suggest to set the estimated ϵ_{oc} for Cimetta to one.

The fitted all-sky parameterizations (Eqs. 9, 10 and 11) result in comparable MEs and RMSEs, indicating that the most important step is the fitting of the parameters, and not the selection of the parameterization. The best performance was produced by the 6th order polynomial, resulting in a ME of less than $1\,\mathrm{W\,m^{-2}}$, in comparison to up to $2.5\,\mathrm{W\,m^{-2}}$ for Eq. (9) and $6\,\mathrm{W\,m^{-2}}$ for Eq. (10) in absolute values. For the RMSE, the differences between the parameterizations are smaller (less than $3\,\mathrm{W\,m^{-2}}$), i.e. the RMSE for all parameterizations scatter around $16\,\mathrm{W\,m^{-2}}$ to $24\,\mathrm{W\,m^{-2}}$ for the low to medium elevation sites, and around $25\,\mathrm{W\,m^{-2}}$ to $32\,\mathrm{W\,m^{-2}}$ for the high elevation sites. The largest RMSE is observed for the parameterization of Eq. (9). When fitting all stations simultaneously, the differences between the MEs is less than one for Eq. (10) and the 6th order polynomial, and the RMSE scatters around $25\,\mathrm{W\,m^{-2}}$. Since the differences between the parameterizations are small, we study the second (modified) parameterization presented in Pirazzini et al. (2001) (i.e. Eq. 10), since this parameterization has been applied by other modelers, is based on physical reasoning,

and includes less parameters than the 6th or 5th order polynomials.

The MEs of the outputs of the Konzelmann parameterization coupled with the cloud emissivity estimation of Eq. (10) range between $-6\,\mathrm{W\,m^{-2}}$ and $2\,\mathrm{W\,m^{-2}}$ (decreasing with increasing elevation) and the RMSEs between $12\,\mathrm{W\,m^{-2}}$ and $22\,\mathrm{W\,m^{-2}}$ (increasing with increasing elevation), when estimating the parameters for each station individually. By fitting all stations simultaneously, the ME ranges between -7 and $6\,\mathrm{W\,m^{-2}}$ and the RMSE ranges between 14 and $25\,\mathrm{W\,m^{-2}}$.

4.2.3 Interpolation of cloud transmissivity during nighttime

The best all-sky LDR results during day- and nighttime were obtained by linearly interpolating the mean of the 4 cloud transmissivities during the last hours in the afternoon preceeding the night, and the 4 h in the following morning. For the simultanoues fitting, it resulted in a ME of around -6 to $7\,\mathrm{W\,m^{-2}}$ (no trend with elevation) and a RMSE between 20 and $35\,\mathrm{W\,m^{-2}}$ (increasing with increasing elevation). Similar results were observed when taking the average of 3 to 5 and 6 h, and for the constant interpolation of a mean of the 5 or 6 preceeding hours. The constant (backward) interpolation by taking one or several values of the following morning did not show reliable output, resulting in MEs of down to $-16\,\mathrm{W\,m^{-2}}$ and RMSEs of up to $40\,\mathrm{W\,m^{-2}}$.

4.2.4 Uncertainty of the all-sky LDR

The uncertainty of the all-sky LDR was estimated by taking the Konzelmann clear-sky parameterization together with the all-sky estimation of Eq. (9). The parameter values come from the fit of all stations simultaneously. The cloud transmissivity was linearly interpolated during nighttime according to the findings in Sect. 4.2.3. The uncertainty is estimated similarly to the uncertainty in the SDR, including the uncertainty of the input variables and the uncertainty of the cloud transmissivity. The parameters (Tables 5 and 6) estimated at all stations simultaneously are varied within their confidence intervals. The 95 %-quantile of the all-sky LDR output uncertainty (Fig. 7) scatters around

Title Page

Abstract | Introduction

Conclusions | References

Tables | Figures

◄ | ►

◄ | ►

Back | Close

Full Screen / Esc

Printer-friendly Version

Interactive Discussion

11 W m^{-2} (increasing with increasing elevation, i.e. 8 W m^{-2} at OTL and 15 W m^{-2} at JUN). In relative terms, the 95 %-quantile of the uncertainty is smaller than 10 % for all time steps, and scatters around 5 %. The mean of the relative uncertainty for the all-sky LDR is around 2.5 %. For further model uncertainty estimations and applications, a conservative estimate of the uncertainty of the all-sky LDR according to Konzelmann et al. (1994) and Pirazzini et al. (2001) is:

$$LDR_{all} = LDR_{all}^{est} \cdot (1 + \varepsilon_{LDR}), \tag{21}$$

with

$$\varepsilon_{LDR_{all}} \sim \mathcal{N}(0, 0.05). \tag{22}$$

A more confident estimate for the uncertainty in the LDR results in

$$\varepsilon_{LDR_{all}} \sim \mathcal{N}(0, 0.025). \tag{23}$$

The function $f(LDR_{all}) = \sigma_{LDR_{all}, rel}$ was fitted through the relative uncertainties of the LDR using non-linear least-squares estimation, which results in:

$$\sigma_{LDR_{all}, rel} = \frac{1}{0.0082 \cdot LDR_{all}^{1.56}} \tag{24}$$

The relative hits of the LDR indicate that for high radiation values (> 300 W m^{-2} for the high elevation sites, and > 400 W m^{-2} for the low elevation sites), the model mostly over-estimates the measurements. For low radiation values, the relative hits reach values of more than 50 % (Fig. 8).

5 Discussion

There are different interesting outcomes that could be discussed here, however we focus the discussion on some specific topics. Since the validation of the presented models has been done previously in other studies (Gueymard, 1993; Marty and Philipona,

2000; Pirazzini et al., 2001; Klok and Oerlemans, 2002; Schillings, 2004), and are in the range of the mentioned studies, we do not focus on the validation in the discussion, but mainly on (1) uncertainties in SDR and LDR parameterizations and their applicability and (2) parameter estimation for the clear- and all-sky LDR.

5.1 Uncertainties in SDR and LDR parameterizations and their applicability

The energy in the atmosphere is a driving factor for any impact study concerned with the energy balance at the Earth's surface. Therefore, many impact models incorporate a parameterization of SDR and LDR in one or another form. Due to the fact that the SDR and LDR can be estimated and studied independently from any successive process at the Earth surface, and can thus be treated as an independent subsystem, the estimated uncertainties for the SDR (Eq. 17) and LDR (Eq. 21) can directly be implemented in any model containing the investigated model formulae. This can be useful for a modeling study including model uncertainties since the estimation of the prior distribution for all input variables and parameters of a complex impact model is time consuming and sometimes difficult, and can be shortened by incorporating the presented results directly. For models containing different SDR and LDR parameterizations, the presented results can either be used as an approximation or reference of the inherent uncertainties, and the estimated prior distributions of parameters and input variables can be used. The functions presented in Eqs. (20) and (24) further allow to differentiate the relative uncertainty in dependence of the amount of radiation.

The comparison of the uncertainties in SDR indicates that they behave similar for the measured (ASRB) and modeled diffuse and global radiation. They range around 15 % for modeled and 10 % for measured diffuse radiation, and 2.5 % for modeled and 2 % for measured global radiation. Similarly, the uncertainty of the measured LDR (2 %) differs not much from the modeled all-sky LDR (2.5 %).

Further, we emphasise that the presented uncertainties are in two ways subjective: a) the selection of the parameters and input variables and b) the prior distributions assigned to them. While a) and b) were estimated as objectively as possible, the reader

should keep in mind that the assumptions taken influence the presented results.

5.2 Parameter estimation for LDR

The fitted clear-sky LDR parameterizations provide better outputs compared to the outputs when applying the parameterizations as they are published. Further, a difference
in performance was observed among the fitted parameterizations, leading to the detection of some best performing parameterization. These results indicate that the key step for modeling the LDR is not mainly the selection of the parameterizations, but rather the fitting of the parameter values to local conditions or the use of a parameterization developed or fitted at the local conditions. By doing so, problems or errors due to wrong
units can be reduced.

For the fitted all-sky parameterization, we have seen that it is not necessary to transform the estimated cloud transmissivity to cloud cover, but the cloud transmissivity can directly be inserted in the all-sky parameterization. Thereby, errors from empirically estimated cloud conversions can be avoided. Similarly as for the clear-sky situation,
fitting the parameterization to local conditions or using parameters estimated at similar locations is a crucial step to obtain reliable results.

6 Conclusions

– For the fixed parameter values (i.e. the mean presented in Table 2), the RMSE scatters around $60 \, \mathrm{W \, m^{-2}}$ for direct, and around $40 \, \mathrm{W \, m^{-2}}$ for diffuse and global
SDR. The negative ME indicate a general under-estimation of direct radiation, which is more pronounced at high elevation sites. In combination with the over-estimation of diffuse radiation, this results in smaller absolute MEs for global radiation, which are even positive for the two low elevation sites Payerne and Locarno Monti, and negative for the higher sites. In general, the global Iqbal radiation
performs satisfyingly.

CC BY

- The uncertainty (as the standard deviation) of the Iqbal SDR, considering input and parameter uncertainty is 20–30 W m^{-2} for direct, 10–25 W m^{-2} for diffuse and around 5–15 W m^{-2} for global radiation when considering solar elevations higher than 30°. In relative terms, the uncertainties for direct go up to 10 %, for diffuse up to 20 % and for global radiation up to 5 %, when estimating the relative uncertainty conservatively. In general, for low sun elevations (and thus low radiation), the uncertainties are larger (in relative terms), and relative hits are few.

- The RMSE of the clear-sky LDR is around 7 W m^{-2} for the best parameterizations (Dilley and O'Brien, 1997; Brutsaert, 1975; Konzelmann et al., 1994), while the ME is almost zero for all parameterizations if the parameterizations are fitted to each station individually. For the simultanous fitting, the ME range between −5 W m^{-2} and 6 W m^{-2}, and the RMSE is less than 12 W m^{-2}.

- Used with Konzelmann et al. (1994), the all-sky parameterization presented in Eq. (8) (Pirazzini et al., 2001) performs best for solar elevation angles greater than zero in order of errors, physical motivation and number of parameters. For the individual fitting, the RMSE scatters around 16 W m^{-2} to 30 W m^{-2}, and the ME from −6 W m^{-2} to 2 W m^{-2} with larger values for lower elevations. Except for the two lowest stations, the all-sky LDR model under-estimates the LDR. The under-estimation at the high locations is coupled to the general under-estimation of the cloud cover, and the respective over-estimation of the cloud transmissivity, which itself is due to the under-estimation of the global radiation at the high locations. However, the errors lie in the range of other all-sky LDR model errors. When estimating all stations simultaneously, the ME ranges between −7 W m^{-2} to 5 W m^{-2}, and the RMSE between 14 W m^{-2} to 25 W m^{-2}.

- The output uncertainty of the all-sky LDR is mostly less than 10 W m^{-2}, and in relative terms it is less than 10 %. A trend with elevation was not observed. In addition, a function indicating the total output uncertainty in dependence of the amount of radiation was estimated for all radiation parameterization.

- The study of the different interpolation techniques of the cloud transmissivity during nighttime has shown that a modeler preferably averages the cloud transmissivity estimated during 4 to 6 h before sunset and after sunrise and then linearly interpolates between these averages. This results in ME of −6 to 7 W m^{-2} and RMSE of 20 to 35 W m^{-2} for the resultant all-sky LDR.

7 Outlook

This study is focussed on the analysis and uncertainty estimation of clear-sky SDR and all-sky LDR parameterizations at seven locations in Switzerland. Estimating the energy fluxes and their uncertainties at locations of potential model input stations is certainly of value for further model applications in nearby locations. However, any model investigating the spatial distribution of a certain phenomenon comprehends diverse formulae to extrapolate the measured input variables. The uncertainties due to these extrapolation techniques such as the lapse rate for temperature was not studied. A further constraint of the presented study is the restriction to examine horizontal locations, neglecting thereby radiation from surrounding terrain and the topographical variability of model outputs and inherent uncertainties. A study investigating these two constraints would certainly deliver additional important information for further model applications.

Appendix A

Clear-sky global SDR

If not otherwise mentioned, all model formulations are from Iqbal (1983).

A1 Solar geometry

In a first step, the solar geometry for each location and time step is estimated according to the geometrical calculations by Corripio (2002). The eccentricity-corrected extraterrestrial solar radiation I_o is obtained by:

$$I_o = \rho \overline{I_o}, \tag{A1}$$

where $\rho \approx \left(\frac{r}{r_0}\right)^2$, where r_0 is the actual and r the mean Sun–Earth distance, is an approximation of the relative distance traversed by the sun ray, and $\overline{I_o} = 1367\,\mathrm{W\,m^{-2}}$ is the solar constant. An approximation for ρ is (Spencer, 1971):

$$\rho = 1.00011 + 0.034221\cos(\phi) + 0.00128\sin(\phi) + 0.000719\cos(2\phi)$$
$$+ 0.000077\sin(2\phi), \tag{A2}$$

where $\phi = 2\pi(d-1)/365$ is the day angle in radians and d is the day of the year.

A2 Direct radiation

The downward broadband SDR is given by

$$SDR_{dir} = 0.9751 I_o \tau_r \tau_w \tau_o \tau_a \tau_g, \tag{A3}$$

where τ_r is the transmittance due to Rayleigh scattering, and τ_w, τ_o, τ_a and τ_g are the transmittances of water vapor, ozone, aerosols and the uniformly mixed gases O_2 and CO_2, respectively.

Attenuation due to dry air particles, aerosols and precipitable water is dependent on the length of the path a solar ray traverses before reaching the ground. Ignoring the Earth's curvature and under the assumption of a horizontal homogeneously distributed atmosphere the relative optical air mass m_r can be estimated as

$$m_r = \frac{1}{\cos\Theta_Z}, \tag{A4}$$

where Θ_Z is the solar zenith angle. Attenuation increases with increasing zenith angle.

Kasten (1966) developed an accurate estimation of the relative optical mass m_r considering the Earth's curvature and the refraction of the real atmosphere:

$$m_r = \frac{1}{cos\Theta_Z + 0.15(93.885 - \Theta_Z)^{-1.253}} . \tag{A5}$$

For non-standard pressures deviating from 1013.25 hPa at sea level, induced by weather or topography, the relative optical air mass m_r is modified to local condition air mass m_a:

$$m_a = m_r \frac{p^*}{1013.25} , \tag{A6}$$

where p^* is screen-level atmospheric pressure (hPa).

Rayleigh scattering transmittance is

$$\tau_r = \exp[-0.0903 m_a^{0.84}(1.0 + m_a - m_a^{1.01})]. \tag{A7}$$

Transmittance by ozone is given by:

$$\tau_o = 1.0 - [0.1611 U_1(1.0 + 139.48 U_1^{-0.3035})$$
$$- 0.002715 U_1(1.0 + 0.044 U_1 + 0.0003 U_1^2)^{-1}], \tag{A8}$$

where $U_1 = l m_r$ is the ozone relative optical path length, and l is the ozone column in cm.

The transmittance by uniformly mixed gases is given by:

$$\tau_g = \exp[-0.0127 m_a^{0.26}], \tag{A9}$$

and the transmittance of water vapor is obtained from:

$$\tau_w = 1 - 2.4959 U_2[(1.0 + 79.034 U_2)^{0.6828} + 6.385 U_2]^{-1}. \tag{A10}$$

Here, $U_2 = w m_r$ is the pressure-corrected relative optical path length of precipitable water. The parameter w denotes the precipitable water (cm).

Aerosol transmittance can be parameterized using a visibility (Iqbal, 1983), and is estimated as proposed by Mächler (1983):

$$\tau_a = (0.97 - 1.265 v^{-0.66}) m_a^{0.9}. \tag{A11}$$

A3 Diffuse radiation

Diffuse radiation is estimated as the sum of the Rayleigh-scattered, the aerosol-scattered and the multiple reflected irradiance, i.e.:

$$SDR_{dif} = SDR_{dif,r} + SDR_{dif,a} + SDR_{dif,rfl}. \tag{A12}$$

The Rayleigh-scattered diffuse irradiance is estimated as

$$SDR_{dif,r} = 0.79 I_o \cos\Theta_z \frac{\tau_o \tau_g \tau_w \tau_{aa} 0.5(1 - \tau_r)}{1 - m_a + m_a^{1.02}}, \tag{A13}$$

where τ_{aa} is the estimated transmittance of direct radiation due to aerosol absorptance:

$$\tau_{aa} = 1 - (1 - \omega_0)(1 - m_a + m_a^{1.06})(1 - \tau_a), \tag{A14}$$

where ω_0 is the single-scattering albedo. We set $\omega_0 = 0.9$ (Bird and Hulstrom, 1980). Diffuse irradiance due to scatttering of aerosols is

$$SDR_{dif,a} = 0.79 I_o \cos\Theta_z \frac{\tau_o \tau_g \tau_w \tau_{aa} 0.84(1 - \tau_{as})}{1 - m_a + m_a^{1.02}}, \tag{A15}$$

where $\tau_{as} = \tau_a / \tau_{aa}$ is the fraction of the incident energy transmitted after scattering effects of aerosols. The between the Earth and the atmosphere multiply-reflected irradiance is

$$SDR_{dif,rfl} = \frac{(SDR_{dir} \cos\Theta_z + SDR_{dif,r} + SDR_{dif,a})\rho_g \rho_a}{1 - \rho_g \rho_a}. \tag{A16}$$

3386

The parameters ρ_g and ρ_a are ground albedo and albedo of the cloudless sky, respectively. The albedo of the cloudless sky is computed as

$$\rho_a = 0.0685 + 0.16(1 - \tau_{as}). \tag{A17}$$

A4 Terrain reflected radiation

The terrain reflection radiation is estimated according to Dozier and Frew (1990):

$$SDR_{ter} = \rho_g \cdot (\frac{1 + \cos(\text{slope})}{2} - \text{svf}) \cdot (SDR_{dir} + SDR_{dif}), \tag{A18}$$

where slope denotes the slope of the simulation point, and svf is the fraction of the sky visible at the simulation point. Since the cos(slope) = 1 and the svf is large (between 0.97 and 1) for all simulation points, the terrain reflected radiation accounts only for a very small part of the global radiation.

A5 Global radiation

Global SDR is the sum of direct SDR (Sect. A2), diffuse radiation (Sect. A3) and the radiation reflected at surrounding terrain (Sect. A4), i.e. $SDR_{glob} = SDR_{dir} + SDR_{dif} + SDR_{ter}$.

Appendix B Estimated ground albedo distributions

The distribution of the ground albedo distribution for each station and each month of the year were estimated according to data from the "MODIS/Terra+Aqua BRDF and Calculated Albedo" dataset.[2]

---

[2]MODIS download information for Cimetta:
Product: MCD43A
Location Centered on: Latitude [46.201], Longitude [8.7908]

Discussion Paper | Discussion Paper | Discussion Paper | Discussion Paper | Discussion Paper

References

Andreas, E. L. and Ackley, S. F.: On the differences in ablation seasons of Arctic and Antarctic sea ice-sheet, J. Atmos. Sci., 39, 440–447, 1982. 3395

Angström, A.: A Study of the Radiation of the Atmosphere, Smithsonian Miscellaneous Collection, 65, 1–159, 1918. 3376, 3395

Bates, D. M. and Chambers, J. M.: Nonlinear Models, Chap. 10, Wadsworth and Brooks/Cole, Pacific Grove, CA, 1992. 3369

Bates, D. M. and Watts, D. G.: Nonlinear Regression Analysis and its Applications, Wiley, New York, 1988. 3369

Beck, M. B.: Water quality modeling: a review of the analysis of uncertainty, Water Resour. Res., 23, 1393–1442, 1987. 3361

Beven, K.: Prophecy, reality and uncertainty in distributed hydrological modelling, Adv. Water Resour., 16, 41–51, 1993. 3361

Bird, R. E. and Hulstrom, R. L.: Direct insolation models, Tech. Report, Solar Energy Research Institute, Colorado, USA, 1980. 3359, 3386

Bird, R. E. and Hulstrom, R. L.: Simplified clear sky model for direct and diffuse insolation horizontal surfaces, Solar Energy Research Institute, Colorado, USA, 1981. 3359

Brunt, D.: Notes on radiation in the atmosphere, Q. J. R. Meteorol. Soc., 58, 389–420, 1932. 3375, 3376, 3395

Size: Approximately 6.5 km wide and 6.5 km high
Time Period: 18 February 2000 to 20 July 2010
Selected Solar Zenith Angle is "local"
Selected Optical Depth is "0.2"

Brutsaert, W.: On a derivable formula for long-wave radiation from clear skies, Water Resour. Res., 11, 742–744, 1975. 3360, 3363, 3376, 3377, 3382, 3395

Cooter, E. and Dhakhwa, G.: A solar radiation model for use in biological applications in the South and Southeastern USA, Agric. Forest Meteorol., 79, 31–51, 1996. 3359

5 Corripio, J. G.: Vectorial algebra algorithms for calculating terrain parameters from DEMs and solar radiation modelling in mountainous terrain, Geogr. Inf. Sci., 17, 1–23, 2002. 3359, 3364, 3384

Crawford, T. M. and Duchon, C. E.: An improved parameterization for estimatin effective atmospheric emissivity for use in calculating daytime downwelling longwave radiation, J. Appl.
10 Meteorol., 38, 474–480, 1998. 3366

Dilley, A. C. and O'Brien, D. M.: Estimating downward clear sky long-wave irradiance at the surface from screen temperature and precipitable water, Q. J. R. Meteorol. Soc., 124a, 1391–1401, 1997. 3365, 3376, 3382, 3395

Dozier, J. and Frew, J.: Rapid calculation of terrain parameters for radiation modeling from
15 digital elevation data, IEEE T. Geosci. Remote, 28, 963–969, 1990. 3387

Dürr, B. and Philipona, R.: Automatic cloud amount detection by surface longwave downward radiation measurements, J. Geophys. Res., 109, D05201, doi:10.1029/2003JD004182, 2004. 3370, 3372

Efimova, N. A.: On methods of calculating monthly values of net long-wave radiation, Meteor.
20 Gidrol., 10, 28–33, 1961. 3395

Erbs, D. G., Klein, S. A., and Duffie, J. A.: Estimation of the diffuse radiation fraction for hourly, daily and monthly-average global radiation, Solar Energy, 28, 293–302, 1982.

Flatau, P. J., Walko, R. L., and Cotton, W. R.: Polynomial fits to saturation vapor pressure, J. Appl. Meteorol., 31, 1507–1513, 1992. 3363

25 Foster, J., Bevis, M., and Raymond, W.: Precipitable water and the lognormal distribution, J. Geophys. Res., 111, D15102, doi:10.1029/2005JD006731, 2006. 3363

Greuell, W., Knap, W. H., and Smeets, P. C.: Elevational changes in meteorological variables along a midlatitude glacier during summer, J. Geophys. Res., 102, 941–954, 1997. 3366

Gruber, S.: Mountain permafrost: Transient spatial modelling, model verification and the use of
30 remote sensing, Ph.D. Thesis, University of Zurich, Zurich, 2005. 3359

Gueymard, C.: Critical analysis and performance assessment of clear sky solar irradiance models using theoretical and measured data, Solar Energy, 51, 121–138, 1993. 3359, 3371, 3379

Title Page

Abstract | Introduction

Conclusions | References

Tables | Figures

|◀ | ▶|

◀ | ▶

Back | Close

Full Screen / Esc

Printer-friendly Version

Interactive Discussion

Gupta, H. V., Beven, K., and Wagener, T.: Model calibration and uncertainty estimation, Ency-
   clopedia of Hydrological Sciences, John Wiley & Sons, 2005. 3361

Hebeler, F. and Purves, R. S.: The impact of parametric uncertainty and topographic error in
   ice sheet modelling, J. Glaciol., 45, 899–919, 2008. 3363

Helbig, N., Löwe, H., and Lehning, M.: Radiosity approach for the shortwave Ssurface radiation
   balance in complex terrain, J. Atmos. Sci., 66, 2900–2912, 2009. 3359

Idso, S. B.: A set of equations for full spectrum and 8 to 14 µm and 10.5 to 12.5 µm thermal
   radiation from cloudless skies, Water Resour. Res., 17, 295–304, 1981. 3376, 3395

Idso, S. B. and Jackson, R. D.: Thermal radiation from the atmosphere, J. Geophys. Res., 74,
   4167–4178, 1969. 3376, 3395

Iqbal, M.: An Introduction to Solar Radiation, Academic Press, Toronto, 1983. 3359, 3360,
   3362, 3363, 3364, 3383, 3386

Iziomon, M. G., Mayer, H., and Matzarakis, A.: Downward atmospheric longwave irradiance
   under clear and cloudy skies: measurement and parameterization, J. Atmos. Solar-Terr.
   Phys., 65, 1107–1116, 2003. 3375, 3395

JCGM: Evaluation of measurement data – Guide to the expression of uncertainty in measure-
   ment, Joint Committee for Guides in Metrology, Bureau International de Poids et Mesures,
   2008. 3368

Kasten, F.: A new table and approximate formular for relative optical air mass, Theor. Appl.
   Climatol., 14, 206–223, 1966. 3385

Kavetski, D., Franks, S. W., and Kuczera, G.: Confronting input uncertainty in environmental
   modeling, Water Sci. Appl. Ser., 6, 49–68, 2003. 3361

Klok, E. J. and Oerlemans, J.: A model study of the energy and mass balance of the Morter-
   atschgletscher, Switzerland, J. Glaciol., 48, 505–518, 2002. 3380

König-Langlo, G. and Augstein, E.: Parameterization of the downward long-wave radiation at
   the Earth's surface in polar regions, Meteorol. Z., 3, 343–347, 1994. 3395

Konzelmann, T., van de Wal, R. S. W., Greuell, W., Bintanja, R., Henneken, E. A. C., and Abe-
   Ouchi, A.: Parameterization of global and longwave incoming radiation for the Greenland
   Ice Sheet, Global Planet. Change, 9, 143–164, 1994. 3360, 3375, 3376, 3377, 3379, 3382,
   3395, 3398, 3405, 3406

Leckner, B.: The spectral distribution of solar radiation at the Earth's surface-elements of
   a model, Solar Energy, 20, 143–150, 1978. 3363

Lhomme, J. P., Vacher, J. J., and Rocheteau, A.: Estimating downward long-wave radiation on

the Andean Altiplano, Agric. Forst Meteorol., 145, 139–148, 2007. 3370

Machguth, H., Purves, R. S., Oerlemans, J., Hoelzle, M., and Paul, F.: Exploring uncertainty in glacier mass balance modelling with Monte Carlo simulation, The Cryosphere, 2, 191–204, doi:10.5194/tc-2-191-2008, 2008. 3359

5 Mächler, M.: Parameterization of solar irradiation under clear skies, Master's Thesis, University of Birtish Columbia, Vancouver, 1983. 3386

Marshunova, M. S.: Principal characteristics of the radiation balance of the underlying surface, Soviet Data on the Arctic Heat Budget and its Climate Influence, Santa Monica, California, USA, 1966. 3395

10 Marty, C. and Philipona, R.: The clear-sky index to separate clear-sky from cloudy-sky situations in climate research, Geophys. Res. Lett., 27, 2649–2652, 2000. 3361, 3379

Maykut, G. A. and Church, P. E.: Radiation climate of Barrow, Alaska, 1962–1966, J. Appl. Meteorol., 12, 620–628, 1973. 3376, 3395

Mulrooney, M. K. and Matney, M. J.: Derivation and application of a global albedo yielding an
15 optical brightness to physical size transformation free of systematic errors, pp. 12–15, 2007. 3364

Okulov, O., Ohvril, H., and Kivi, R.: Atmospheric precipitable water in Estonia, 1990–2001, Boreal Environ. Res., 7, 291–200, 2002. 3362

Oreopoulos, L. and Davies, R.: Plane parallel albedo biases from satellite observations. Part II:
20 Parameterizations for bias removal, Am. Meteorol. Soc., 11, 933–944, 1998. 3364

ORNL DAAC: Oak Ridge National Laboratory Distributed Active Archive Center, MODIS subsetted land products, Collection 5, ORNL DAAC, Oak Ridge, Tennessee, USA, 2010, available at: http://daac.ornl.gov/MODIS/modis.html, last access: March 2010. 3364

Philipona, R., Fröhlich, C., and Betz, Ch.: Characterization of pyranometers and the accuracy
25 of atmospheric longwave radiation measurements, Appl. Opt., 34, 1598–1605, 1995. 3361

Philipona, R., Marty, C., Fröhlich, C., and Heimo, A.: Measurements of the longwave radiation budget in the Alps, in IRS 96: Current Problems in Atmospheric Radiation, edited by: Smith, W. L. and Stamnes K., A. Deepak Publishing, Hampton, Virginia, USA, 786–789, 1996. 3361

Pirazzini, R., Nardino, M., Orsini, A., Calzolari, F., Georgiadis, T., and Levizzani, V.: Param-
30 eterization of the downward longwave radiation from clear and cloudy skies at Ny Alesund (Svalbard), in IRS 2000: Current Problems in Atmospheric Radiation, edited by: Smith, W. L. and Timofeyev, Y. A., A. Deepak Publishing, Hampton, Virginia, 559–562, 2001.

Plüss, C. and Ohmura, A.: Longwave radiation on snow-covered mountainous surfaces, J. Appl.

Meteorol., 36, 818–824, 1997. 3366, 3367, 3375, 3377, 3379, 3380, 3382

Prata, A. J.: A new long-wave formula for estimating downward clearsky radiation at the surface, Q. J. R. Meteorol. Soc., 122, 1127–1151, 1996. 3375, 3395

Reitan, C.: Surface dew point and water vapor aloft, J. Appl. Meteorol., 2, 776–779, 1963. 3363, 3395

Satterlund, D. R.: An improved equation for estimating longwave radiation from the atmosphere, Water Resour. Res., 15, 1649–1650, 1979. 3363

Schillings, C.: Bestimmung langjähriger stündlicher Zeitreihen und räumlich hochaufgelöster Karten der Direkt-Normal-Strahlung auf der Basis von Meteosat-Daten und Atmosphärenparametern für die Nutzung in konzentrierenden Solarkraftwerken, Ph.D. thesis, Philipps-Universität Marburg, Marburg, 2004. 3395

Spencer, J. W.: Fourier series representation of the position of the Sun, Search, 2, 172, 1971. 3359, 3380, 3402

Staehelin, J., Renaud, A., Bader, J., McPeters, R., Viatte, P., Hoegger, B., Bugnion, V., Giroud, M., and Schill, H.: Total ozone series at Arosa (Switzerland): Homogenization and data comparison, J. Geophys. Res., 103, 5827–5841, 1998. 3384

Swinbank, W. C.: Long-wave radiation from clear skies, Q. J. R. Meterol. Soc., 89, 330–348, 1963. 3363

Yamamoto, G.: On nocturnal radiation, Sci. Rep. Tohoku Universitiy, 2, 27–43, 1950. 3395

Zillman, J. and Commonwealth Bureau of Meteorology (Australia): A study of some aspects of the radiation and heat budgets of the Southern Hemisphere oceans, Meteorological Study, Canberra: Australian Government Publishing Service, 1972. 3395

3395

Table 1. Meta data of the MeteoSwiss stations. At each place, one ANETZ and one ASRB station is located.

Location	Abbreviation	Lat (deg N)	Long (deg E)	Ele [m]
Locarno-Monti	OTL	46.1726	8.7874	367
Payerne	PAY	46.8116	6.9424	490
Davos	DAV	46.813	9.8435	1590
Cimetta	CIM	46.201	8.7908	1672
Weissfluhjoch	WFJ	46.8333	9.8064	2690
Gornergrat	GOR	45.9832	7.7845	3130
Jungfraujoch	JUN	46.5474	7.9853	3580

Table 2. Input, model parameters and validation data with uncertainty distributions, mean μ and standard deviation σ. Note that the distribution for the ANETZ and ASRB measurements concern the precision (error) of the measurement (denoted with E), whereas the distribution in the parameters (except for m_r) concerns the parameter value itself. Since ground albedo varies temporally and spatially, its distribution is estimated for each station and each month seperately (Table 7).

	Measurement	Distribution	μ	σ	Range	Unit	Symbol
Input	Air temperature	Normal (E)	0	0.2		K	T^*
	Relative humidity	Normal (E)	0	5	[0,100]	%	h_r^*
	Air pressure	Normal (E)	0	0.2		hPa	p^*
Parameter	Ozone column	Lognormal	314	38		DU	l
	Visibility	Normal	60	21	[5,120]	km	v
	PrecWatConstant	Lognormal	47	0.38		$g\,K\,cm^{-2\,hPa^{-1}}$	a_w
	Rel. opt. air mass	Normal (E)	0	0.03			m_r
	Ground Albedo	Lognormal			[0,1]		ρ_g
Validation	Global SDR	Normal (E)	0	2 %		$W\,m^{-2}$	I_{glob}^*
	Diffuse SDR	Normal (E)	0	10 %		$W\,m^{-2}$	I_{dif}^*
	LDR	Normal (E)	0	2 %	$W\,m^{-2}$	LDR_{in}^*

Table 3. Parameterizations of clear-sky emissivity. p_v is the water vapour pressure [hPa], and T the measured temperature [K]. x_1, x_2 and x_3 denote the statistical parameters.

Publication	Abbr.	ϵ_{cl}	x_1	x_2	x_3
Maykut and Church (1973)	may	x_1	0.7855		
König-Langlo and Augstein (1994)			0.765		
Angström (1918)	angs	$x_1 - x_2 \cdot 10^{-0.067 \cdot p_v}$	0.83	0.18	
Brunt (1932); Yamamoto (1950)	brun	$x_1 + x_2 \cdot p_v^{x_3}$	0.51	0.066	0.5
Marshunova (1966)			0.67	0.05	0.5
Efimova (1961)			0.746	0.0066	1
Swinbank (1963)	swin	$x_1 \cdot 10^{-6} \cdot T^{*x_2}$	9.365	2	
Zillman (1972)			9.2	2	
Idso and Jackson (1969)	jack	$1 - x_1 \cdot \exp(-x_2 \cdot 10^{-4} \cdot (273 - T^*)^2)$	0.261	7.77	
Brutsaert (1975)	brut	$x_1 \cdot (\frac{p_v}{T^*})^{1/x_2}$	1.24	7	
Konzelmann et al. (1994)	konz	$0.23 + x_1 \cdot (\frac{100 p_v}{T^*})^{1/x_2}$	0.484	8	
Plüss and Ohmura (1996)			0.642	7	
Satterlund (1979)	satt	$x_1 \cdot (1 - \exp(-p_v^{\frac{T^*}{2016}}))$	1.08		
Idso (1981)	idso	$x_1 + x_2 \cdot 10^{-5} \cdot p_v \cdot \exp(\frac{x_3}{T^*})$	0.7	5.95	1500
Andreas and Ackley (1982)			0.601	5.95	1500
Iziomon et al. (2003)	izio	$1 - x_1 \cdot \exp(-11.5 \cdot \frac{p_v}{T^*})$	0.43		
Prata (1996)	prat	$1 - (1 + x_1 \cdot (\frac{p_v}{T^*})) \cdot \exp(-(1.2 + 3 \cdot x_1 \cdot \frac{p_v}{T^*})^{x_2})$	46.5	0.5	
Dilley and O'Brien (1997)	dill	$(x_1 + x_2 \cdot (\frac{T^*}{273.16})^6 + x_3 \cdot (\frac{465 \frac{p_v}{T}}{25})^{0.5})/(\sigma_{SB} T^{*4})$	59.38	113.7	96.96

Table 4. Validation of the SDR. The model simulation was performed using the mean values of the parameters and the input variables (Table 2). The unit of RMSE and ME is $\mathrm{W\,m^{-2}}$.

	Direct			Diffuse			Global		
	RMSE	ME	R^2	RMSE	ME	R^2	RMSE	ME	R^2
OTL	57	−15	0.95	48	28	0.43	33	13	0.99
PAY	52	−13	0.96	46	23	0.45	25	11	0.99
DAV	59	−31	0.96	40	23	0.43	37	−9	0.99
CIM	54	−36	0.97	39	24	0.49	24	−12	0.99
WFJ	64	−48	0.97	39	18	0.46	46	−30	0.98
GOR	66	−50	0.98	38	11	0.46	49	−39	0.99
JUN	78	−35	0.94	39	11	0.42	64	−24	0.97

Table 5. Values of the fitted parameters of the clear-sky LDR parameterizations to the seven locations. Empty spaces denote parameterizations for which the non-linear least squares algorithm did not converge. The first column indicates the published parameter values, the second column indicates the estimated parameters when all stations are treated simultaneously.

	Pub	All	OTL	PAY	DAV	CIM	WFJ	GOR	JUN
may_1	0.7855	0.67	0.74	0.76	0.71	0.69	0.63	0.61	0.59
$angs_1$	0.83	0.83	0.81	0.81	0.8	0.79	0.79	0.78	0.8
$angs_2$	0.18	0.28	0.21	0.18	0.17	0.19	0.25	0.25	0.28
$brun_1$	0.51	−0.0689	−0.12	0.56	0.5	−0.47	0.13	−0.03	
$brun_2$	0.066	0.65	0.74	0.1	0.14	1.08	0.45	0.6	
$brun_3$	0.5	0.105	0.08	0.3	0.26	0.05	0.12	0.09	
$swin_1$	9.365	0.85	752.36	17631.61	7627.6	7.84	1.46	3.86	10.77
$swin_2$	2	2.42	1.22	0.67	0.81	2.02	2.32	2.14	1.95
$jack_1$	0.261	0.35	0.29	0.25	0.29	0.33	0.36	0.38	0.4
$jack_2$	7.77	6.08	4.58	2.37	1.05	10.74	−4.82	−5.5	−5.05
$brut_1$	1.24	1.13	1.05	1.03	1	1	1	0.96	0.97
$brut_2$	7	8.35	10.48	11.7	12.12	11.49	10.12	10.78	10.5
$konz_1$	0.484	0.97	0.85	0.82	0.8	0.8	0.84	0.79	0.81
$konz_2$	8	5.46	7.2	8.14	8.2	7.66	6.38	6.65	6.39
$satt_1$	1.08	0.97	1.01	1.03	1.01	0.99	0.94	0.91	0.91
$idso_1$	0.7	0.55	0.64	0.63	0.61	0.62	0.55	0.54	0.52
$idso_2$	5.95	0.47	0.5	0.07	0.05	3.93	1.86	3.48	3.65
$idso_3$	1500	2396	2239.84	2835.31	2967.02	1652.28	1986.77	1833.69	1850.15
$izio_1$	0.43	0.4	0.36	0.34	0.35	0.38	0.42	0.44	0.45
$prat_1$	46.5	717	98.5	20.42	158.63	242.69	874.27	1169.56	1589.56
$prat_2$	0.5	0.36	0.44	0.57	0.42	0.39	0.35	0.35	0.34
$dill_1$	59.38	26.24	57.7	66.62	62.13	35.68	28.46	27.95	23.13
$dill_2$	113.7	124.72	114.87	90.83	96.27	141.41	127.66	125.97	129.39
$dill_3$	96.96	122.02	101.98	129.63	123.7	77.03	100.22	98.49	100.85

Title Page

Abstract | Introduction

Conclusions | References

Tables | Figures

|◄ | ►|

◄ | ►

Back | Close

Full Screen / Esc

Printer-friendly Version

Interactive Discussion

Table 6. Fitted parameters of the all-sky LDR parameterizations presented in Eqs. (9) and (10). The clear-sky emissivity is estimated according to Konzelmann et al. (1994). The first line consists of the estimates when all stations are fitted simultaneously.

	$\tilde{a}$	$\tilde{p}_0$	ϵ_{oc}	$\tilde{p}_1$	$\tilde{p}_2$
All	0.31	0.86	0.944	3.83	3.22
OTL	0.28	1.44	0.94	0.26	0.36
PAY	0.31	1.26	0.97	3.17	2.47
CAV	0.29	0.93	0.97	1.73	1.66
CIM	0.36	0.97	1.01	1.21	1.24
WFJ	0.41	0.67	0.97	3.87	3.42
GOR	0.29	0.32	0.77	0.64	1.34
JUN	0.47	0.51	0.93	1.42	1.98

Table 7. Mean and standarddeviation ($\mu|\sigma$) of the ground albedo from the "MODIS/Terra+Aqua BRDF and Calculated Albedo" data set, estimated at each location for a surrounding terrain of approximately 6.5^2 km^2 for each month of the year.

Month	CIM	DAV	GOR	JUN	OTL	PAY	WFJ
Jan	0.20|0.13	0.39|0.19	0.29|0.20	0.16|0.09	0.11|0.07	0.20|0.13	0.50|0.15
Feb	0.16|0.10	0.43|0.19	0.51|0.21	0.30|0.19	0.11|0.05	0.16|0.06	0.64|0.13
Mar	0.13|0.06	0.42|0.18	0.57|0.11	0.50|0.19	0.10|0.04	0.15|0.01	0.63|0.12
Apr	0.12|0.02	0.33|0.19	0.54|0.11	0.36|0.15	0.10|0.04	0.17|0.01	0.54|0.15
May	0.13|0.01	0.15|0.09	0.30|0.16	0.30|0.12	0.11|0.04	0.17|0.01	0.31|0.19
Jun	0.14|0.01	0.12|0.03	0.18|0.06	0.27|0.10	0.11|0.04	0.16|0.01	0.16|0.04
Jul	0.13|0.01	0.11|0.02	0.15|0.04	0.26|0.11	0.11|0.04	0.16|0.01	0.14|0.02
Aug	0.13|0.02	0.11|0.02	0.14|0.04	0.24|0.11	0.11|0.04	0.16|0.01	0.14|0.02
Sep	0.13|0.02	0.12|0.07	0.15|0.06	0.20|0.10	0.11|0.04	0.16|0.01	0.17|0.11
Oct	0.13|0.03	0.16|0.14	0.17|0.10	0.17|0.11	0.11|0.04	0.15|0.01	0.24|0.19
Nov	0.14|0.07	0.28|0.20	0.20|0.15	0.16|0.12	0.11|0.05	0.14|0.04	0.45|0.20
Dec	0.19|0.13	0.35|0.18	0.16|0.08	0.12|0.06	0.11|0.06	0.15|0.09	0.55|0.16

Full Screen / Esc

Printer-friendly Version

Interactive Discussion
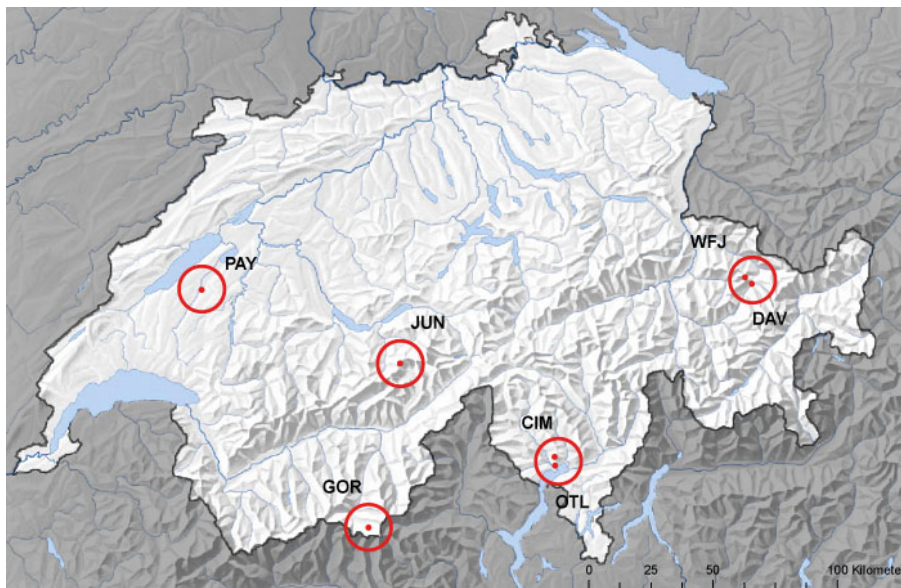
Fig. 1. Locations of the seven MeteoSwiss stations in Switzerland (geodata © swisstopo). The coordinates of the locations are from MeteoSwiss (http://www.meteoswiss.admin.ch).
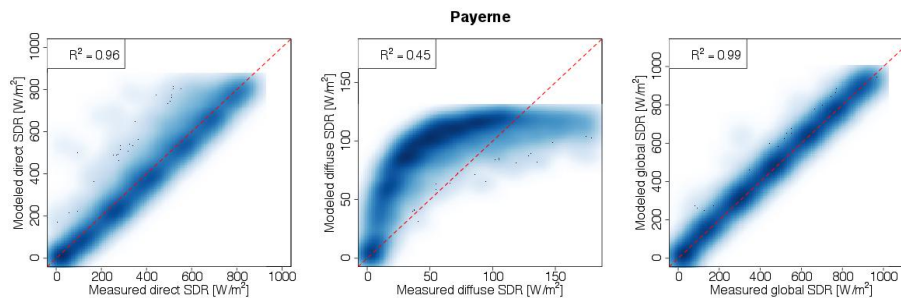
Fig. 2. Smoothed scatter plots of direct, diffuse and global modeled and measured SDR at Payerne. The dashed red line indicates the perfect fit.
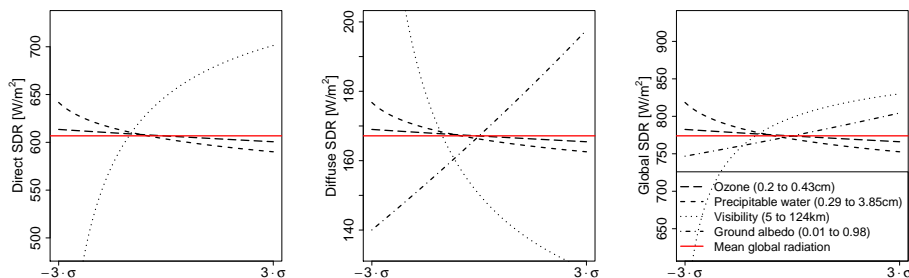
Fig. 3. Local sensitivities of direct, diffuse and global SDR to ozone, precipitable water, visibility and ground albedo (diffuse and global only), adapted according to Schillings (2004, Fig. 3.9). The sensitivities are estimated for constant path length $m_r = 4.3$, the mean value at Jungfraujoch. The range of the different parameters are given in the legend. The slope of the different curves reflect the relative sensitivity to each parameter. The mean SDR is indicated in red. The x-range is $\mu - 3\sigma$ to $\mu + 3\sigma$ (cf. Table 2).
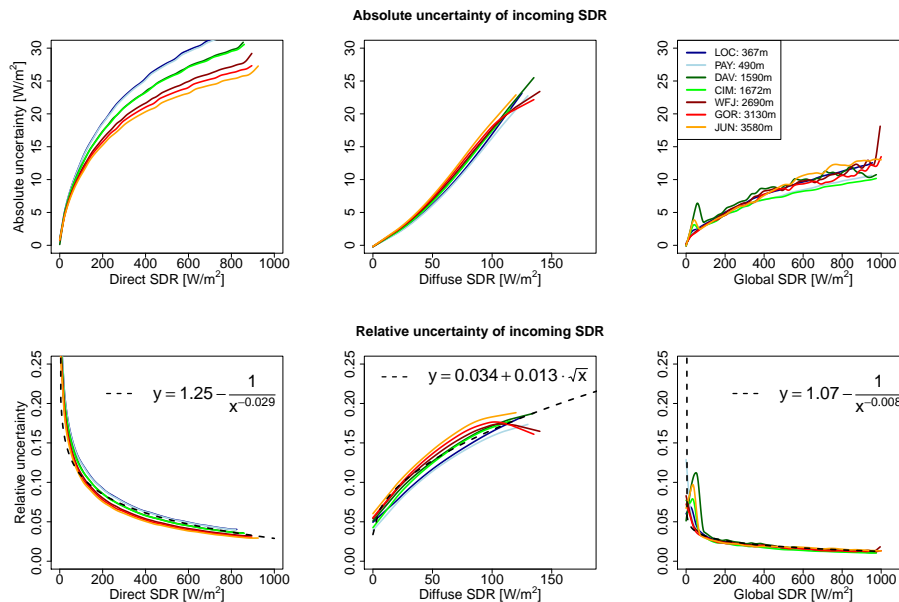
Fig. 4. Smoothed mean lengths of the standard deviation of clear-sky direct, diffuse and global SDR, as a function of radiation [$W\,m^{-2}$]. The graphs were obtained by estimating the mean standard deviation of each $5\,W\,m^{-2}$ radiation interval. Smoothing was performed using non-parametric regression. The dashed black line denotes the fit of the function $f(SDR) = \sigma_{SDR,rel}$, where $x := SDR_i$ and $y := \sigma_{SDR_i,rel}$. The coefficients of the function $f(x) = y$ were obtained by non-linear least-squares regression.
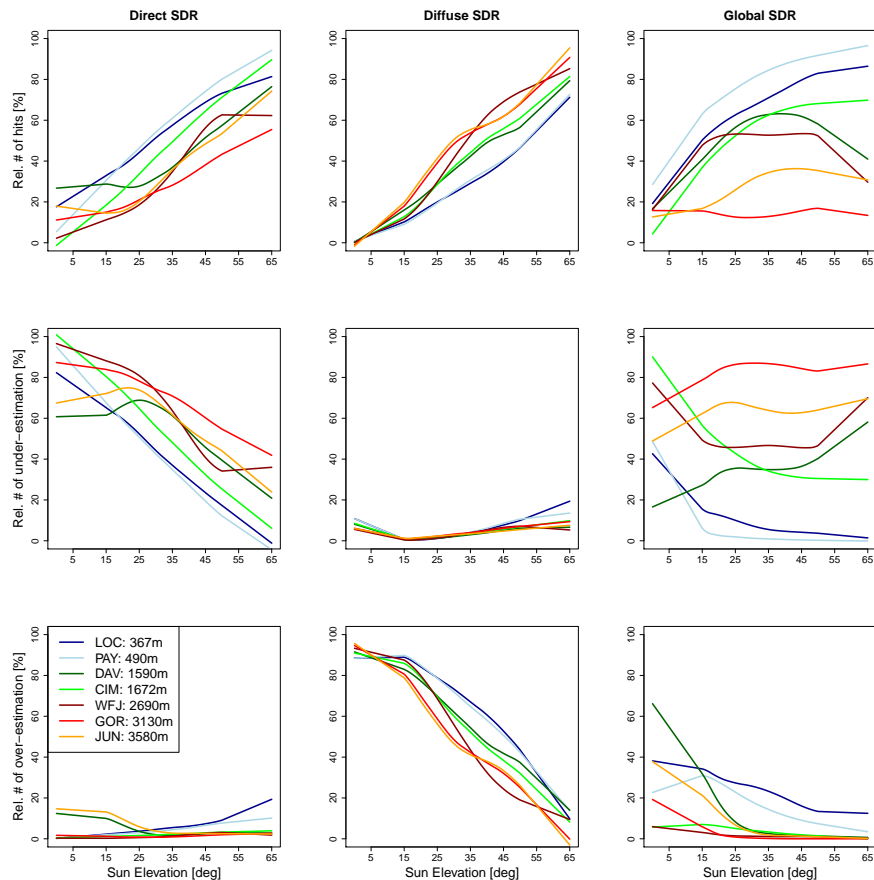
Fig. 5. Relative number of hits for of direct (left column), diffuse (middle column) and global (right column) SDR in % in dependence of the solar elevation (upper row). The middle row shows the relative number of radiation measurements that are under-estimated by the model, the lowest row shows the number of over-estimated values.

Title Page

Abstract | Introduction

Conclusions | References

Tables | Figures

◄◄ | ►►

◄ | ►

Back | Close

Full Screen / Esc

Printer-friendly Version

Interactive Discussion
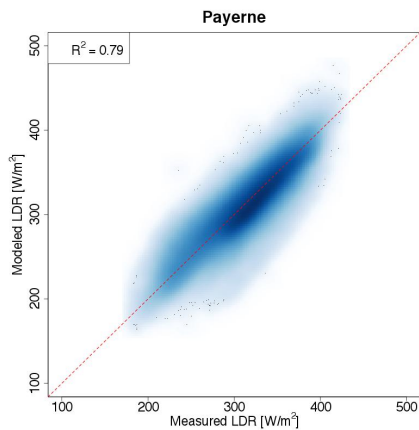
Fig. 6. Smoothed scatter plot of measured and modeled all-sky LDR during day- and nighttime according to Konzelmann et al. (1994) and Eq. (9).
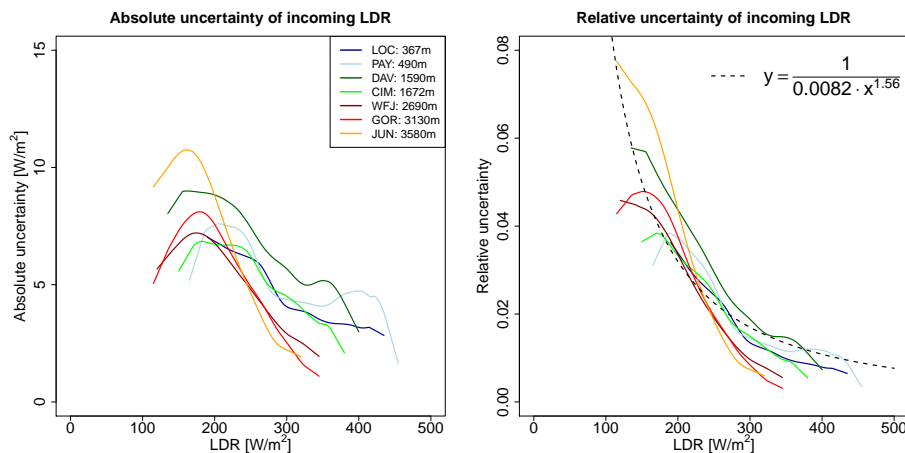
Fig. 7. Absolute and relative uncertainty of the modeled LDR. The clear-sky emissivity is estimated according to Konzelmann et al. (1994), and the all-sky parameterization is found in Eq. (9). The dashed black line denotes the fit of the function $f(\text{LDR}) = \sigma_{\text{LDR,rel}}$, where $x := \text{LDR}$ and $y := \sigma_{\text{LDR,rel}}$.
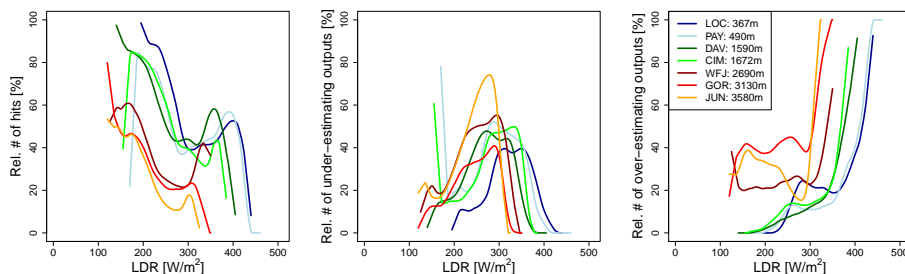
Fig. 8. Relative hits (left figure) of the modeled LDR as a function of the mean modeled LDR. The figures on the right show the relative number of under- resp. over-estimated measurements.